J Mater Sci: Mater Electron (2017) 28:14696–14701
DOI 10.1007/s10854-017-7337-0

The role of sintering conditions on the superconducting parameters of MgB_2

Salem A. S. Qaid[1,2] · Nasser S. Alzayed[1] · M. Shahabuddin[1] · Shahid M. Ramay[1] · Shahid Atiq[3]

Received: 27 April 2017 / Accepted: 9 June 2017 / Published online: 16 June 2017

Abstract In this paper, we report the performance of MgB_2 superconductor prepared in a wide range of sintering temperatures. Pristine MgB_2 superconductor was prepared under the same conditions in one batch. The sintering temperatures are optimized to get the best superconducting parameters enhancing, especially critical current density. It was found that a low sintering temperature enhanced critical current density at the high magnetic region. Approximately the opposite of this effect was found in case of high sintering temperature. Crystallites size was increased with increasing of sintering temperature. It was found that smaller the crystallite size, higher was the value of critical current density. In addition, a slight increase in transition temperature was also observed as the sintering temperature was increased. High upper critical field values obtained at low sintering temperature were attributed to the strong grain boundary defects.

✉ Salem A. S. Qaid
salemqaid@gmail.com

✉ Nasser S. Alzayed
nalzayed@ksu.edu.sa

[1] Department of Physics and Astronomy, College of Science, King Saud University, P.O. Box 2455, Riyadh 11451, Saudi Arabia

[2] Department of Physics, Faculty of Applied Science, Thamar University, Thamar, Yemen

[3] Centre of Excellence in Solid State Physics, University of the Punjab, Lahore, Pakistan

1 Introduction

Superconducting properties of MgB_2 were discovered first time in 2001. Among binary metallic compound superconductors, it shows the highest transition temperature ($T_c = 39\,°C$) [1]. This material possesses some unique properties for example, a nearly anisotropic superconducting behavior, high ductility, robustness against grain boundaries [2] and allowing a reasonable mechanical deformation. This makes MgB_2 more suitable for applications over high T_c cuprates or pnictides-based superconductors. Since the discovery of superconductivity in MgB_2, much effort has been made to enhance the magnetic characteristics of this material. The flux pinning and subsequent enhancement of critical current density (J_c), in MgB_2 were reported in numerous works using chemical doping. On the other hand, a very few attempts have been made to improve MgB_2 performance based on optimizing heat treatment conditions which play a vital role in homogenizing the grain shapes and sizes [3–6]. In addition, J_c could be limited by many factors. Some of these reasons have been discussed in detail in literature [5]. However, the synthesis conditions and the parameters play a significant role to overcome the limitation of J_c in polycrystalline MgB_2. One of the most important synthesis factors is the sintering temperature which controls the particle growth mechanism. This factor could easily be tuned to get rid of impurity phases which in turn affected the superconducting parameters.

In this context, the present work focuses on tuning the sintering temperatures in a wide range to get the best enhancement in grain connectivity (A_F, the effective cross section), J_c and critical fields for bulk MgB_2 synthesized from amorphous nano-boron powder. After structural investigation, a comprehensive investigation has been conducted to correlate the measured superconducting parameters.

2 Experimental details

The amorphous nano-boron powder (Pavezyum Advanced Chemicals, >98%) was used in the present work to synthesize the samples. Pristine MgB_2 samples were synthesized by standard solid state reaction method. The stoichiometric amounts of both the ingredients were ball-milled for 4 h using a Planetary micro mill (PULVERISETTE 7 premium line, FRITSCH). The resulting powder was pressed into pellets using a hydraulic press by applying a force of 4 ton. These pellets were wrapped in tantalum foils and put in the iron container. The heating process was performed in a tube furnace under the flow of a high purity argon gas to reduce the oxidation of Mg. The heating rate and time duration were chosen to be 5 °C/min and 30 min, respectively [5]. A batch of four samples was synthesized using the same conditions. The samples were subsequently sintered at 650, 750, 850 and 950 °C for 30 min each, and were tagged as P-1, P-2, P-3 and P-4, respectively. The crystal structure of the prepared samples was confirmed using a Rigaku Ultima IV, X-ray diffractometer (XRD). MAUD software was used to analyze different phases and to confirm the lattice parameters. Physical properties measurement system (PPMS), QUANTUM DESIGN (MODEL6000), together with its attached vibrating sample magnetometer, were used to obtain the magnetic hysteresis (M–H) loops. J_c was obtained from M–H loops using Bean's critical state model [7]. A four-wire resistance measurements technique and PPMS system was combined to obtain the resistivity data, from which irreversible field (B_{irr}), upper critical field (B_{c2}), and T_c were evaluated.

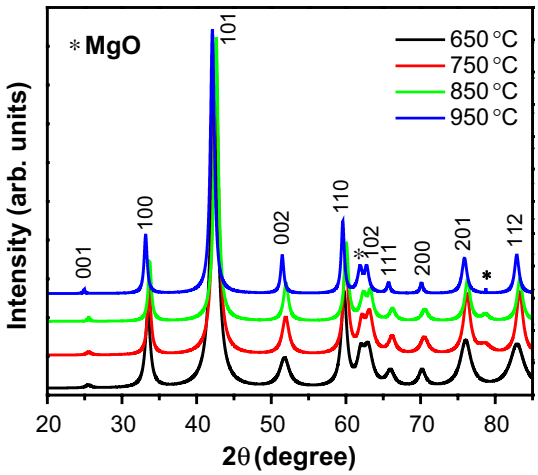

Fig. 1 XRD patterns of all the samples sintered at 650, 750, 850 and 950 °C. The indexed peaks belong to MgB_2. * indicates the peaks emerging from (220) and (222) planes of MgO

3 Results and discussion

Figure 1 shows the diffraction patterns of all the samples sintered at 650, 750, 850 and 950 °C for 30 min. The patterns reveal that all the samples possess hexagonal crystal structure with space group P6/mmm, as majority of the strong peaks present in all the patterns were perfectly matched with ICSD # 00-038-1369, a characteristic reference pattern of MgB_2. It was also observed that the peak width was gradually decreased as the sintering temperature was increased which subsequently decreased the full width at half maximum (FWHM). In addition to the peaks corresponding to the MgB_2 phase, some impurity peaks related to MgO (ICSD # 00-045-0946) were also witnessed. However, these were very low intensity peaks emerging from (220) and (222) planes, appearing around 2θ values of 62.14° and 78.75°, respectively. The data obtained from diffraction was analyzed in detail via Rietveld's refinement using a MAUD software. The lattice parameters (*a* & *c*), *c*/*a* ratio, the fraction percentage ratio of MgO to MgB_2, the fractional densities of these two components and their ratio were determined, as shown in Table 1. The data reveals that within the estimation error, the values of MgO weight (wt%) and volume (vol%) ratio are around 10%, which agrees well with Kim et al. [5]. Although the samples sintered at different temperatures show different fractional percentage ratio of MgO to MgB_2, the overall fraction is estimated around ~10% [5, 6]. Density ratio (D_r) of MgO, of the P-1 sample is a bit high as compared to the other samples, yet it is the closest to the theoretical value. The closeness of this value to the theoretical values indicates the quality of the samples. The shift of the diffraction angles and hence the peak positions with varying the sintering temperature is depicted in terms of the variation in lattice constants and change in *c*/*a* ratio [8], as shown in

Table 1 Lattice parameters, crystallites size (D_p) and weight (wt%) & volume (vol%) percentage ratio of MgO to pure MgB_2 samples sintered at 650, 750, 850 and 950 °C. D_r is the density ratio: D_{MgO} / D_{MgB2}

Sample	S.T. (°C)	*a* (Å)	*c* (Å)	*c*/*a*	D_p (Å)	MgO		D_r	D_r
						wt%	vol%		error%
P-1	650	3.096	3.533	1.141	095.53	09.59	07.23	1.361	0.023
P-2	750	3.090	3.528	1.142	122.35	14.22	10.91	1.354	0.028
P-3	850	3.090	3.532	1.143	141.92	10.46	07.94	1.354	0.028
P-4	950	3.086	3.528	1.143	147.72	04.46	03.34	1.352	0.029

Fig. 2. Ignoring the effect of strain on FWHM, the crystallites size (D_P), was calculated using Scherrer's formula [9];

$$D_P = \frac{0.94\lambda}{\beta_{1/2}cos\theta} \quad (1)$$

where λ is the wavelength of CuK_α radiation, $\beta_{1/2}$ is FWHM of the most intense peak in the diffraction patterns

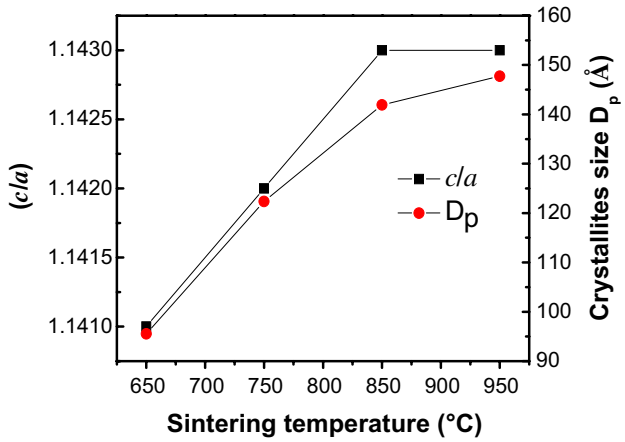

Fig. 2 Variation of (*c*/*a*) ratio and crystallites size (D_p) against sintering temperature for MgB_2 samples sintered at 650, 750, 850 and 950 °C

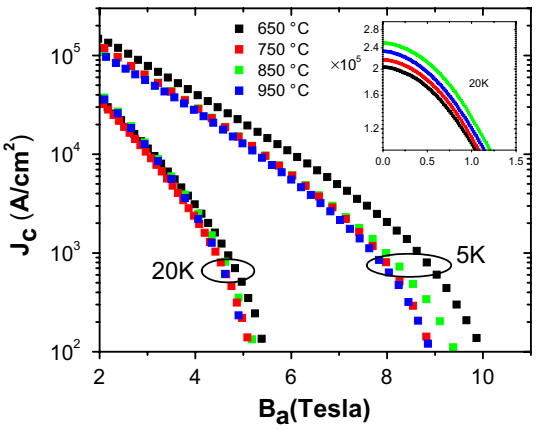

Fig. 3 Critical current density (J_c) vs applied magnetic field (B_a) at 5 and 20 K for the different sintering temperatures for MgB_2 samples

measured in radians, and θ is the peak position in degrees. As evident by Fig. 2, the *c*/*a* ratio and D_P increase as the sintering temperature increases. This behavior is in agreement with some earlier reports [10]. Moreover, the increasing value of D_p with increasing sintering temperature is expected due to the increase of density [10]. It has been reported in the literature that smaller the grain size, the quality of MgB_2 superconductors is enhanced [11, 12]. This statement is further confirmed when the performance of MgB_2 samples is compared on the basis of enhancement in J_c.

The variation in J_c as a function of applied magnetic field (B_a), for all the samples sintered at different temperatures is shown in Fig. 3. The J_c measurements were made at two different temperatures, i.e., 5 and 20 K in B_a range of 0 to 10 T. The trend as depicted by the curves shows a strong dependence of J_c on B_a at both the temperatures. It is evident that J_c decreases with increase in B_a for both the temperatures. However, at low B_a, the sample sintered at 650 °C gives the best J_c enhancement when the measurements were made at 5 K. On the other hand, at low fields, this sample gives the least J_c values when the measurement was made at 20 K, as shown in the inset of Fig. 3. B_{irr} was obtained when the J_c degraded to 100 A/cm^2. Its values behave as that of J_c at high magnetic fields. Table 2 shows the measured values of J_c and B_{irr} at the measurement temperatures of 5 and 20 K and at B_a values of 0 and 4 T, for every sintering temperature.

At measurement temperature of T = 20 K and applied magnetic field, B_a = 0 T, the best enhancement of J_c is observed for the sample sintered at 850 °C (P-3), as shown in the inset of Fig. 3 and listed in Table 2. For both, T = 5 and 20 K, the lowest value of B_{irr} is observed for the sample sintered at 950 °C (P-4). This behavior can be attributed to decrease of flux pinners at the grain boundaries. The origin of flux pinning center is the impurities that are located at the grain boundaries. As the crystallite size was increasing, the volume of grain boundary impurities was minimized [6] and hence resulted in a decrease of B_{irr}.

The behavior of the resistivity against temperature (from 5 to 45 K) at different applied magnetic fields (0 to 13 T) and vice versa was also determined by combining the PPMS measurements with four point probe technique. Figure 4

Table 2 Critical current density (J_c) and irreversible magnetic field (B_{irr}) at the measurement temperature (T = 5 and 20 K), and applied magnetics fields (B_a = 0 and 4 T)

Sample	J_c (0 T, 20 K) × 10^5 A/cm^2	J_c (4 T, 20 K) × 10^3 A/cm^2	B_{irr} (Tesla) (10^2 A/cm^2, 20 K)	J_c (0 T, 5 K) × 10^5 A/cm^2	J_c (4 T, 5 K) × 10^4 A/cm^2	B_{irr} (Tesla) (10^2 A/cm^2, 5 K)
P-1	2.03	3.07	5.42	1.15	4.11	9.96
P-2	2.16	2.32	5.17	1.52	2.99	8.93
P-3	2.50	2.75	5.23	1.71	3.04	9.43
P-4	2.33	2.46	5.06	1.69	2.76	8.91

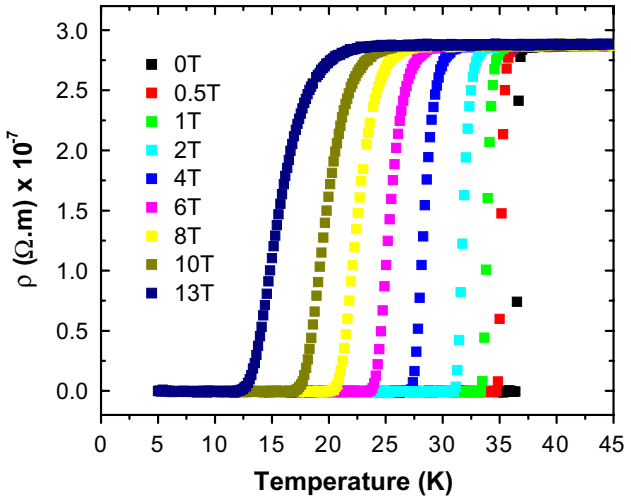

Fig. 4 The temperature dependence of resistivity for the MgB_2 sample sintered at 650 °C (P-1)

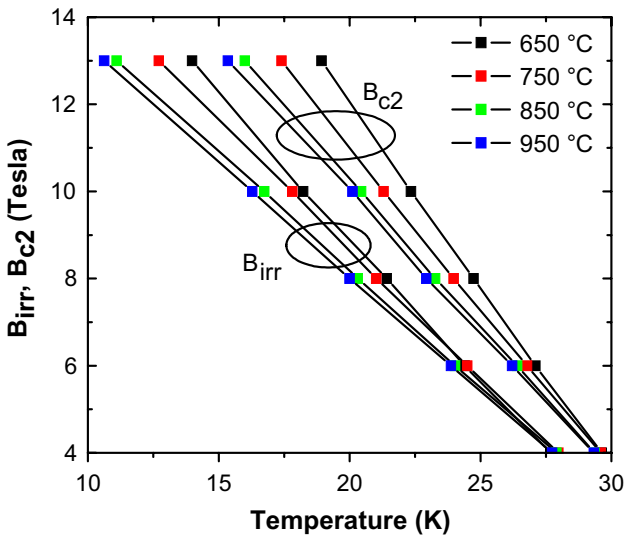

Fig. 5 Temperature dependence of B_{c2} and B_{irr} for the MgB_2 samples sintered at 650, 750, 850 and 950 °C

shows the temperature dependence of resistivity for the MgB_2 sample sintered at 650 °C. Table 3 shows the onset and offset transition temperatures for different applied magnetic fields, ranging from 0 to 13 T. The ΔT_c values are calculated from: $\Delta T_c = T_{c2} - T_{c1}$; where T_{c2} and T_{c1} are the onset and offset transition temperatures, respectively.

The curves in Fig. 4 reveal how the transition temperatures decrease as the applied magnetic field increases. The behavior is also evident from the values listed in Table 3. The upper transition temperature, T_{c2} varies from ~37 to ~22 K as the applied magnetic field increases from 0 to 13 T. This point can be explained in view of critical magnetic fields, i.e. B_{c2} and B_{irr}. B_{c2} and B_{irr} were taken when the resistivity dropped to 90 and 10% of its normal value, respectively. Figure 5 shows the temperature dependence of B_{c2} and B_{irr} for the MgB_2 samples sintered at 650, 750, 850 and 950 °C for 30 min.

The trends indicate a clear dependence of sintering temperature on the superconducting parameters. In order to further elaborate this tendency, let us start by discussing the dependence of resistivity, ρ, of the samples on the temperature, T, and the applied magnetic field. Figure 6 shows the trend of the resistivity against temperature at zero applied magnetic field, for the MgB_2 samples, sintered at 650, 750, 850 and 950 °C for 30 min.

As shown in Table 4, the transition temperature increased with increase of sintering temperature. This

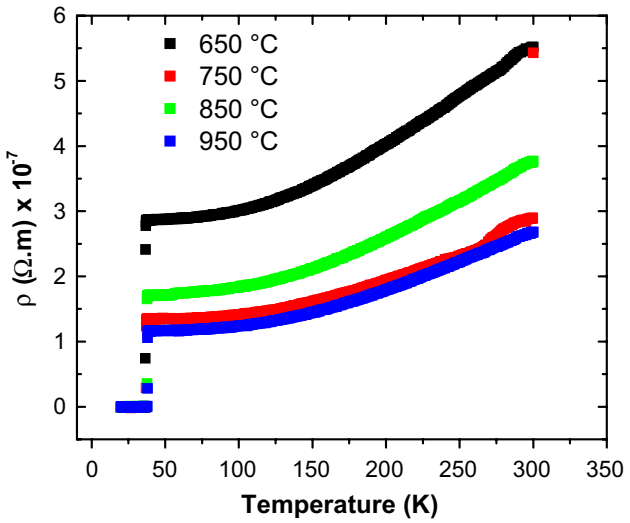

Fig. 6 The plot of the resistivity vs temperature for the MgB_2 samples sintered at 650, 750, 850 and 950 °C. The measurements are taken under no magnetic field

behavior is in accordance with that already reported in the literature [9]. The change in critical transition temperature (ΔT_c) is maximum for the samples sintered at 750 °C as compared to all the other samples in series,

Table 3 The onset and offset transition temperature for different applied magnetic fields for the pure MgB_2 sample sintered at 650 °C (P-1)

B_a (T)	0	0.5	1	2	4	6	8	10	13
T_{c1} (K)	36.60	36.14	35.00	33.61	31.38	27.67	24.4	21.42	18.22
T_{c2} (K)	36.91	36.46	35.58	34.54	32.61	29.63	27.10	24.73	22.34
ΔT_c (K)	0.31	0.32	0.58	0.93	1.23	1.96	2.70	3.31	4.12

Table 4 Superconducting parameters for the MgB_2 samples sintered at 650, 750, 850 and 950 °C. The measurements are taken at zero magnetic field

Sample	S.T (°C)	T_{c1} (K)	T_{c2} (K)	ΔT_c (K)	$\Delta\rho\times10^{-7}$ (Ωm)	RRR (R_{300}/R_{Tc2})	Connectivity A_f ($\Delta\rho_{sc}/\Delta\rho)\times100\%$	$B_{c2}(0)$ (T)
P-1	650	36.60	36.91	0.31	2.66	2.13	23.78	21.92
P-2	750	36.82	37.22	0.40	1.56	4.45	40.64	23.18
P-3	850	37.70	37.84	0.14	2.05	2.46	30.90	19.18
P-4	950	37.85	38.11	0.26	1.51	2.54	41.80	17.50

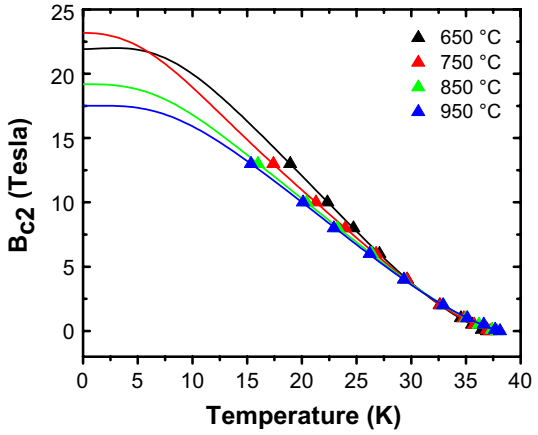

Fig. 7 Temperature dependence of the upper critical field for MgB_2 samples. The symbols are for experimental data whereas the solid lines are for the Ginzburg–Landau equation fitting

with equal interval of sintering temperature. A careful look at the ρ–T curves reveals that the sample sintered at 850 °C has the most sharpness in curve, means the lowest ΔT_c. The ρ value at the temperature, T_{c2} was known as residual resistivity (RR) and the ratio R_{300}/R_{Tc2} is the residual resistivity ratio. The most factors affecting the grain connectivity, A_F, are the grain size and the amount of the impurities located at the grain boundaries. Increase in sintering temperature leads to the growth of new MgB_2 grains and hence enhancing the A_F values [13, 14]. However, growing MgO phase leads to depress the A_F [8]. Considering this fact, the behavior of A_F can be interpreted if its values were correlated to XRD quantitative analysis, as given in Table 4. The crystallite size was maximum for the sample sintered at 950 °C and the least MgO phase fraction was noted, hence high A_F was the result. The increasing of MgO wt% in P-2 sample as compared to P-1 led to depress A_F. On the other hand, for P-3 and P-4 samples, the D_P increases while MgO wt% decreases, resulting in increased A_F values. Correlating the J_c enhancements, it is noted that the minimal decrease of A_F was found for P-1, which was correlated with the maximal critical currents [15]. The values of critical fields at low temperatures can be estimated by fitting the experimental data of B_{c2} versus T, using curve fitting. There are few expressions which need to be used to do the fitting [16, 17]. The Ginsburg–Landau method is more appropriate in the present case [18]. The expression involved is shown in Eq. 2.

$$B_{c2}(T) = \frac{B_{c2}(0)\theta^{1+a}}{1-(1+\alpha)\omega + l\omega^2 + m\omega^3} \quad \text{with } \omega = (1-\theta)\theta^{1+a} \text{ and } \theta = 1 - {}^{T}/_{T_c} \tag{2}$$

where α, l and m are fitting parameters. This equation has been used to find B_{c2} at low temperatures by fitting the experimental data of critical field with operator temperature [9]. Applying this method to experimental data of all the MgB_2 samples sintered at various temperatures, the fitted curves obtained are shown in Fig. 7.

The B_{C2} values at 0 K are obtained from the intercept of the fitted curve lines with B_{c2} axis of Fig. 7. These values are shown in Table 4. It is noted that the B_{C2} (0) values of the samples P-1 and P-2 are higher as compared to the remaining samples. This is attributed to the strong grain boundary defects resulting by sintering at relatively low temperatures as reported earlier [19]. In other words, the similarity of B_{c2} behavior with that of MgO wt% confirms that the presence of MgO makes grain boundary defects more prominent, thus enhancing the critical fields.

4 Conclusion

The performance of MgB_2 superconductor samples, prepared at different sintering temperatures under the same conditions in one batch, has been investigated. Among all samples, the sample sintered at 650 °C for 30 min, exhibited small crystallite sizes and grain connectivity but higher J_c values. Temperature dependence of B_{c2} showed that the samples that were sintered at low temperature, namely 650 and 750 °C gave better B_{c2} enhancement as compared to those sintered at high temperatures, namely 850 and 950 °C. It is inferred from B_{c2} behavior that sintering at low temperature leads to strong grain boundary defects. A slight increase in transition temperature with the increase of sintering temperature was also observed.

Acknowledgements This project was supported by King Saud University, Deanship of Scientific Research, College of Science, Research Center.

References

1. J. Nagamatsu, N. Nakagawa, T. Muranaka, Y. Zenitani, J. Akimitsu, Nature **410**, 63–64 (2001)
2. D.C. Larbalestier, L.D. Cooley, M.O. Rikel, A.A. Polyanskii, J. Jiang, S. Patnaik, X.Y. Cai, D.M. Feldmann, A. Gurevich, A.A. Squitieri, M.T. Naus, C.B. Eom, E.E. Hellstrom, R.J. Cava, K.A. Regan, N. Rogado, M.A. Hayward, T. He, J.S. Slusky, P. Khalifah, K. Inumaru, M. Haas, Nature **410**, 186–189 (2001)
3. A. Yamamoto, J.I. Shimoyama, S. Ueda, Y. Katsura, S. Horri, K. Kishio, Supercond Sci Technol **18**, 116 (2005)
4. C.U. Jung, M.S. Park, W.N. Kang, M.S. Kim, K.H.P. Kim, S.Y. Lee, S.I. Lee, Appl Phys Lett **78**, 4157–4159 (2001)
5. J.H. Kim, S.X. Dou, J.L. Wang, D.Q. Shi, X. Xu, M.S.A. Hossain, W.K. Yeoh, S. Choi, T. Kiyoshi, Supercond Sci Technol **20**, 448 (2007)
6. J.H. Kim, S.X. Dou, D.Q. Shi, M. Rindfleisch, M. Tomsic, Supercond Sci Technol **20**, 1026 (2007)
7. C.P. Bean, Phys Rev Lett **8**, 250–253 (1962)
8. D.K. Sing, B. Tiwari, R. Jha, H. Kishan, V.P.S. Awana, Phys C **505**, 104–108 (2014)
9. A. Vajpayee, R. Jha, A.K. Srivastava, H. Kishan, M. Tropeano, C. Ferdeghini, V.P.S. Awana, Supercond Sci Technol **24**, 045013 (2011)
10. R. Islam, M.O. Rahman, M.A. Hakim, D.K Saha, S. Saiduzzaman, S. Noor, M. Al-Mamun, Mater Sci Appl **3**, 326–331 (2012)
11. G. Giunchi, G, Ripamonti, S. Raineri, D. Botta, R. Gerbaldo, R. Quarantiello, Supercond Sci Technol **17**, S583 (2004)
12. K. Onar, Y. Balci, M.E. Yakinci, J Mater Sci **25**, 2104–2110 (2014)
13. X. Xu, J.H. Kim, S.X. Dou, S. Choi, J.H. Lee, H.W. Park, M. Rindfleish, M.T. Less, J Appl Phys **105**, 103913 (2009)
14. Y. Takano, H. Takeya, H. Fujii, H. Kumakura, T. Hatano, K. Togano, Appl Phys Lett **78**, 2914–2916 (2001)
15. K. Husekova, I. Husek, P. kovac, M. Kulich, E. Dobrocka, V. Strbik, Phys C **470**, 331–335 (2010)
16. L. Guang-Tong, J. Hao, L. Zheng, G. Hong-Xia, C. Guang-Can, J. Duo, S. Lian-Feng, X. Si-Shen, L. Jian-Lin, Chin Phys Lett **25**, 687 (2008)
17. K.H. Muller, G. Fuchs, A. Handstein, K. Nenkov, V.N. Narozhnyi, D. Eckert, J Alloy Compd **322**, L10–L13 (2001)
18. I.N. Askerzade, A. Gencer, N. Guclu, Supercond Sci Technol **15**, L13 (2002)
19. W.K. Yeoh, J. Horvat, J.H. Kim, X. Xu, S.X. Dou, Appl Phys Lett **90**, 122502 (2007)